Atmospheric Research 99 (2011) 579–589

Contents lists available at ScienceDirect

Atmospheric Research

journal homepage: www.elsevier.com/locate/atmos

An operational MODIS aerosol retrieval algorithm at high spatial resolution, and its application over a complex urban region

Man Sing Wong [a], Janet E. Nichol [a,*], Kwon Ho Lee [b]

[a] Department of Land Surveying and Geo-Informatics, The Hong Kong Polytechnic University, Hung Hom, Kowloon, Hong Kong
[b] Department of Satellite Geoinformatics Engineering, Kyungil University, Gyungsangbukdo, Korea

ARTICLE INFO

Article history:
Received 3 May 2009
Received in revised form 9 November 2010
Accepted 13 December 2010

Keywords:
Aerosols
Air pollution
MODIS
Remote sensing

ABSTRACT

Aerosol retrieval algorithms for the MODerate Resolution Imaging Spectroradiometer (MODIS) have been developed to estimate aerosol and microphysical properties of the atmosphere, which help to address aerosol climatic issues at global scale. However, higher spatial resolution aerosol products for urban areas have not been well-researched mainly due to the difficulty of differentiating aerosols from bright surfaces in urban areas. Here, an aerosol retrieval algorithm using the MODIS 500-m resolution bands is described, to retrieve aerosol properties over Hong Kong and the Pearl River Delta region. The rationale of our technique is to first estimate the aerosol reflectances by decomposing the top-of-atmosphere reflectances from surface reflectances and Rayleigh path reflectances. For the determination of surface reflectances, a Minimum Reflectance Technique (MRT) is used, and MRT images are computed for different seasons. For conversion of aerosol reflectance to aerosol optical thickness (AOT), comprehensive Look Up Tables specific to the local region are constructed, which consider aerosol properties and sun-viewing geometry in the radiative transfer calculations. Four local aerosol types, namely coastal urban, polluted urban, dust, and heavy pollution, were derived using cluster analysis on 3 years of AERONET measurements in Hong Kong. The resulting 500 m AOT images were found to be highly correlated with ground measurements from the AERONET ($r^2 = 0.767$) and Microtops II sunphotometers ($r^2 = 0.760$) in Hong Kong. This study further demonstrates the application of the fine resolution AOT images for monitoring inter-urban and intra-urban aerosol distributions and the influence of trans-boundary flows. These applications include characterization of spatial patterns of AOT within the city, and detection of regional biomass burning sources.

1. Introduction

The retrieval of atmospheric aerosol amounts from satellite images has been attempted for three decades (Otterman and Fraser, 1979; Tanré et al., 1979; Deschamps et al., 1980). The basic aim is to retrieve the spectral information about the atmosphere from the path between the surface and satellite (Kaufman et al., 1997a,b; Kaufman and Tanré, 1998; King et al., 1999; Lee et al., 2009). This is complex because ground surface reflectances are difficult to distinguish from the total satellite received signal. Thus, the estimation of surface reflectances is the key factor in aerosol retrieval, with the aerosol component being the residual.

Since the estimation of surface reflectance is easier over dark surfaces, Kaufman et al. (1997a,b) first identified dark pixels in the mid-Infrared channel of the MODerate Resolution Imaging Spectroradiometer (MODIS) satellite sensor and estimated their reflectance at 470 and 660 nm. This is known as the Dense Dark Vegetation (DDV) method (Kaufman et al., 1997a,b; Kaufman and Tanré, 1998). The DDV algorithm (later known as MODIS operational collection 4 algorithm) works on the different aerosol scattering properties of the different wavelengths, with lower scattering by longer

* Corresponding author. Tel.: +852 2766 5952.
E-mail address: lsjanet@polyu.edu.hk (J.E. Nichol).

0169-8095/$ – see front matter © 2010 Elsevier B.V. All rights reserved.
doi:10.1016/j.atmosres.2010.12.015

wavelengths. The algorithm removes 20% of the darkest pixels and 50% of the brightest pixels within 10 km kernels, and the remaining pixels are retained to represent aerosol over dark targets, after cloud effects and surface inhomogeneities have been removed (Kaufman and Tanré, 1998). Chu et al. (2002) observed that the MODIS collection 4 (DDV) algorithm had a positive bias in comparison to the AErosol Robotic NETwork (AERONET) sunphotometer data (Holben et al., 1998), and some inherent problems in determining surface reflectance using the DDV algorithm were reported by Remer et al. (2005) and Levy et al. (2004). Therefore, Levy et al. (2007) developed collection 5, which modifies the surface reflectance determination by considering the band correlation based on vegetation index ($NDVI_{SWIR}$) and the scattering angle. The new collection 5 data have been shown to have significant improvements in aerosol optical thickness (AOT) retrievals in China (Mi et al., 2007; Li et al., 2007). However, there remain several major limitations of MODIS aerosol products for local/urban scale study, including the following: (i) it does not retrieve over bright surfaces such as urban and heterogeneous areas, (ii) the heterogeneous nature of urban surfaces complicates the derivation of surface reflectances, and (iii) the 10 km spatial resolution is too coarse to characterize purely local aerosol plumes.

In order to extract the aerosol component from top-of-atmosphere (TOA) reflectances over a wider range of surfaces, a surface reflectance database was developed based on the Minimum Reflectance Technique (MRT). This technique composites the lowest reflecting pixels over a time series of co-registered images to create the minimum reflectance image over that time period. Herman and Celarier (1997) used the MRT technique for TOMS data, and Koelemeijer et al. (2003) used it with GOME data. In view of the coarse resolution, the accuracy of AOT (within 30% of AERONET ground measurements (Hsu et al., 2004)) could be considered good. However, the 10 km spatial resolution of the MODIS products only provide meaningful depictions on a broad regional scale, whereas aerosol monitoring over complex regions, such as urban areas in Hong Kong (1095 km^2), requires more spatial and spectral detail to pinpoint local sources. Li et al. (2005) developed a 1 km AOT algorithm based on the MODIS collection 4 algorithm for a study in Hong Kong, but it was limited to dense vegetated areas and validated using handheld sunphotometers over non-urban surfaces only. In order to retrieve and map aerosol distributions over urban areas with a high level of detail, a MODIS 500 m resolution aerosol retrieval algorithm, which uses the MRT technique, is described here.

2. Study area and data used

Hong Kong, a commercial and financial city located in southeast China (Fig. 1), has suffered serious air pollution for the last decade due largely to rapid urban and industrial expansion of the cities of the neighboring Pearl River Delta (PRD) region of mainland China. Thousands of polluting factories, forty-five power plants, and thousands of construction sites are concentrated within a small spatial extent due to massive urbanization over the last decade. The socio-economic activities of Hong Kong and Macau, situated on opposite sides of the PRD, are directly affected by such changes.

Data collected by the Hong Kong PolyU AERONET station (22.3 lat, 114.2 lon) since its establishment in 2005 show aerosol levels to be high, compared with other urban stations worldwide, with an annual mean AOT of 0.69 at 440 nm, compared with 0.57 for Beijing, 0.55 for Singapore, 0.22 for Rome, and 0.24 for Goddard Space Flight Center.

For retrieving the AOT at 500 m resolution, the 470, 550, and 660 nm wavebands of the TERRA/MODIS level 1B calibrated reflectance (MOD02HKM) were collected. In addition, the 10 km resolution MODIS aerosol products (MOD04) and the 1 km resolution surface reflectance product (MOD09) were collected for comparison purposes. The retrieved AOT images were validated by comparison with the Hong Kong AERONET station and Microtops II sunphotometer measurements. A total of 172 Microtops II sunphotometer measurements was taken on Nov. 11, 2007; Nov. 28, 2007; Dec. 14, 2007, from 9:00 a.m. to 12:00 p.m. Measurements were taken at 10-min intervals within ± 30-min

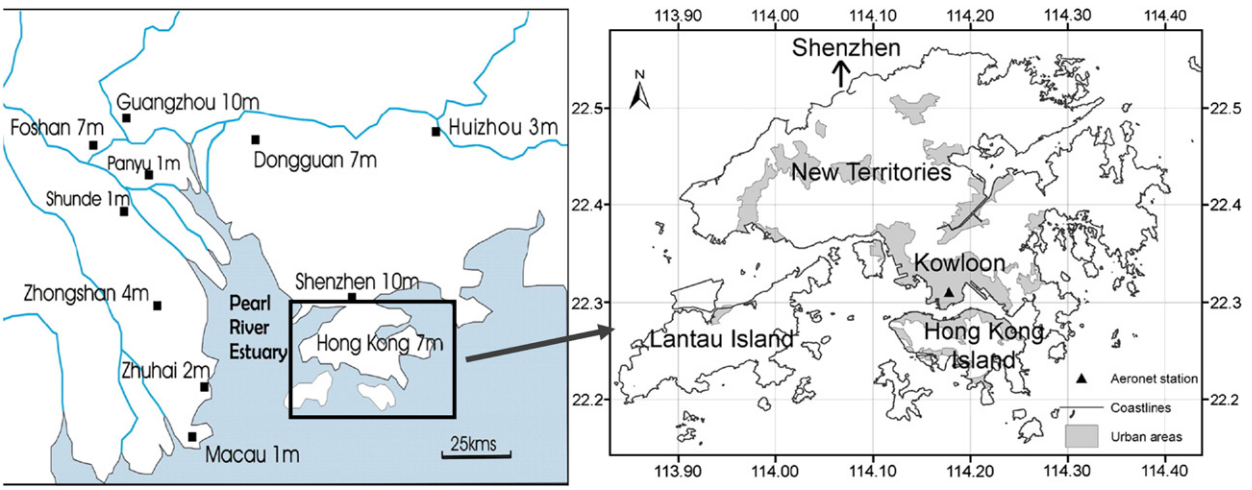

Fig. 1. Hong Kong and cities of Pearl River Delta region, with population size (millions). Urban areas in Hong Kong and location of the AERONET station are shown.

MODIS of the overpass time, and they were averaged. The Microtops II measurements were quality controlled by adopting the Microtops II land protocol and sharp sun targeting during the observations. This gives 14 temporally matched measurements at 14 different sites, including bright urban surfaces, urban grass, and rural areas. The typical error between multiple Microtops II instruments was within 1% to 2% and the uncertainty of AOT is 0.03–0.05 AOT (wavelength-dependent), which was cross-validated with Hong Kong PolyU AERONET station.

The AErosol RObotic NETwork, AERONET (Holben et al., 1998), is a federated network of ground sunphotomers, of which there are over 400 sites around the world. An AERONET station consists of a Cimel sunphotometer, which measures the aerosol extinction using multiple wavelengths, a solar panel, and a controller. It provides real-time aerosol optical thickness, precipitable water, inversion products including size distribution, single scattering albedo, and refractive index based on the solutions of radiative transfer equations. The uncertainty of AOT calibration for the AERONET sunphotometer is 0.01–0.02 AOT according to wavelength, and the Microtops II sunphotometers were calibrated annually with the AERONET sunphotometer. Although Ichoku et al. (2002) assume a 50-km distance from an AERONET ground station to be acceptable for validating the 10 km resolution collection 4 and 5 data at global scale, there is no established protocol for higher resolution; therefore, we adopted more rigorous standards by using only the 500 m pixel corresponding to AERONET.

3. Methodology

A whole year (2007) of TERRA/MODIS 500 m resolution data (470, 550, 660 nm) was used for aerosol retrieval over Hong Kong using the Minimum Reflectance Technique. The rationale of the MRT algorithm is to determine the aerosol reflectance by decomposing the top-of-atmosphere (TOA) reflectance from surface reflectance and the Rayleigh path

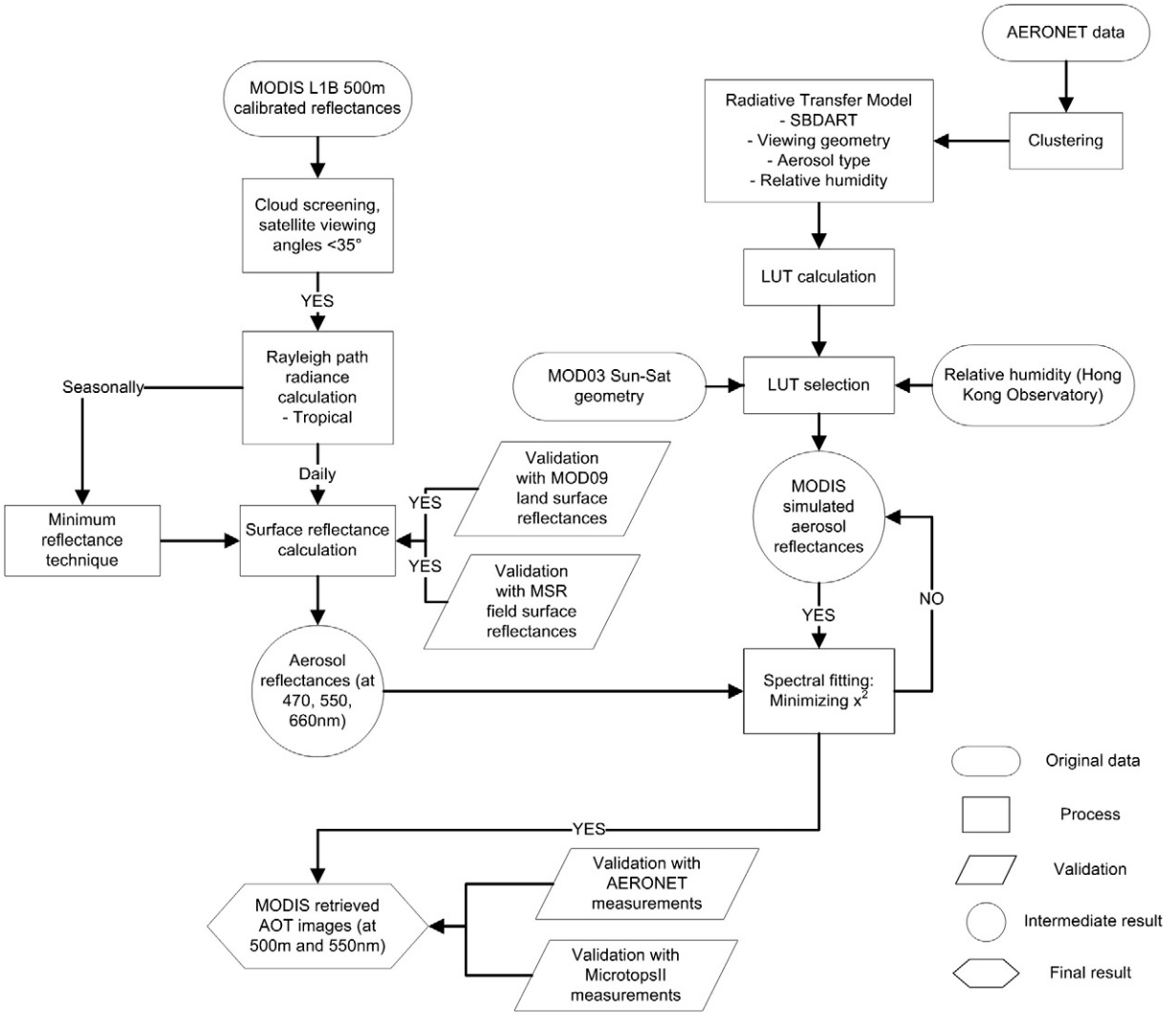

Fig. 2. Methodology for aerosol retrieval in the study.

reflectance. The TOA reflectance ρ_{TOA} is expressed as (Kaufman et al., 1997a,b):

$$\rho_{TOA} = \rho_{Aer} + \rho_{Ray} + \frac{\Gamma_{Tot}(\theta_0)\cdot\Gamma_{Tot}(\theta_s)\cdot\rho_{Surf}}{1-\rho_{Surf}\cdot r_{Hem}} \quad (1)$$

where θ_0 and θ_s are sun and satellite zenith angle. ρ_{Aer}, ρ_{Ray}, ρ_{Surf} are aerosol, Rayleigh, and surface reflectance. $\Gamma_{Tot}(\theta_0)$ and $\Gamma_{Tot}(\theta_s)$ are total atmospheric transmittances, containing both direct and diffuse transmission for sun illumination and satellite viewing geometry. The total transmittances include Rayleigh scattering and aerosol extinction, which can be given as $\Gamma_{Tot} = \Gamma_{Ray}\cdot\Gamma_{Aer}\cdot r_{Hem}$ is the hemispheric reflectance. Fig. 2 illustrates the work flow of aerosol retrieval in this study.

Firstly, the AERONET data (2005 to 2008) from the Hong Kong PolyU station were acquired and clustered to four different aerosol models. The aerosol models coupled with different viewing geometries were input into a radiative transfer model to build Look Up Tables (LUTs) (more descriptions in Section 3.2). To minimize computer memory usage, the LUT geometry was interpolated to the specific satellite geometry. The simulated aerosol reflectances and TOA reflectances as a function of AOT were then created.

Secondly, the MODIS 500 m calibrated reflectance images in 2007 were acquired from NASA Goddard Earth Science Distributed Active Archive Center. Geometric correction, reprojection, cloud and water screening, view angle screening, and Rayleigh correction were applied to the images. The Minimum Reflectance Technique was then applied to the MODIS 500 m images to create surface reflectance images. The Minimum Reflectance Technique composites the lowest reflecting pixels over a time series of co-registered images (e.g., 3 months) to create the minimum reflectance image over that time period. In order to validate the surface reflectance derived from the MRT, the MODIS surface reflectance products (MOD09 8-day composite surface reflectance images at 1 km resolution) were acquired. This product has been validated with 150 AERONET stations worldwide and is considered acceptable if the data error lies within $\pm 0.005 + 0.05 \cdot \rho$ (ρ is surface reflectance) (Vermote and El Saleous, 2006). Fifty-one ground-based reflectance measurements using Cropscan MSR-16R multispectral radiometer (MSR) were taken on four winter dates: Oct. 21, 2006; Oct. 29, 2006; Nov. 05, 2006; and Dec. 29, 2006. It is assumed that vegetation does not change much in terms of reflectance in winter, thus these ground measurements were used to validate the results from the winter MRT image. The general uncertainty of MSR data is ca. 0.005 reflectance units (Chang et al., 2005).

Thirdly, the aerosol reflectances derived from Eq. (1) were compared with modeled aerosol reflectances from LUTs using a spectral fitting technique. The aerosol model with the minimum residual was then selected and the corresponding AOT values were obtained for the 500 m images at 550 nm.

Finally, the derived AOT images were compared with AERONET and Microtops II sunphotometer measurements. Statistical estimators including correlation coefficient, root mean square (RMS), and mean absolute differences (MAD) were used to examine the accuracy.

3.1. Surface reflectance

Atmospheric path radiance is composed of Rayleigh and aerosol radiances and their multiple scattering interactions. Once the Rayleigh reflectances have been estimated, a surface reflectance database can be derived based on the minimum reflectance technique (more descriptions of Rayleigh reflectance are given in the Appendix). To minimize seasonal land cover changes over the time series of MRT images, seasonal minimum reflectance images were derived based on at least thirty clear-sky images for each of four seasons, and images with satellite viewing angles larger than 35° were removed. Then the second minimum reflectance values (rather than the actual minimum) were retrieved in order to avoid abnormal low reflectance such as noise or shadow (Wong et al., 2008; Wong, 2009). It was noted that the second minimum reflectance values have a stronger agreement with the surface reflectances. In addition, clouds were removed by threshold-

Table 1
Summary of the cluster analysis results, including AOT (τ_{500}), 4 single scattering albedo values, 2 real and imaginary refractive index values, angstrom exponent ($\alpha_{870-440}$) value, asymmetry factor (676 nm) value, 2 mean radius values, 2 standard deviation values, 2 mode total volume values, and number of records for four different aerosol types.

	Coastal urban	Polluted urban	Dust	Heavy pollution
Aerosol optical thickness (500 nm)	0.451	0.518	0.510	1.065
Single scattering albedo (439 nm)	0.876	0.869	0.885	0.894
Single scattering albedo (676 nm)	0.889	0.874	0.871	0.911
Single scattering albedo (869 nm)	0.878	0.857	0.855	0.899
Single scattering albedo (1020 nm)	0.872	0.844	0.848	0.888
Real refractive index (676 nm)	1.470	1.452	1.500	1.452
Imaginary refractive index (676 nm)	0.014	0.022	0.016	0.015
Angstrom coefficient (870/440 nm)	1.363	1.316	0.952	1.286
Asymmetry factor (676 nm)	0.643	0.665	0.683	0.682
Fine mode total volume ($\mu m^3/\mu m^2$)	0.064	0.081	0.070	0.155
Fine mode mean radius (μm)	0.181	0.222	0.262	0.244
Geometric standard deviation (fine)	0.478	0.562	0.644	0.542
Coarse mode total volume ($\mu m^3/\mu m^2$)	0.055	0.038	0.148	0.066
Coarse mode mean radius (μm)	2.458	3.177	4.484	2.892
Geometric standard deviation (coarse)	0.672	0.592	0.504	0.594
Number of records (%)	332 (45%)	216 (30%)	22 (3%)	160 (22%)

ing the visible wavebands, which is essential in cloud-prone areas like Hong Kong. Since there is no high-resolution thermal band in MODHKM (500 m) data, a tailor-made cloud-masking algorithm was devised to make use of three visible channels and a NDVI band. This algorithm tests the brightness of reflectance for each pixel, with thresholds based on a trial-and-error approach (Eq. (2)):

$$\text{If (reflectance at 470 nm} > 0.2\text{) or (reflectance at 550nm} > 0.2\text{) or (reflectance at 660 nm} > 0.2\text{) or (NDVI} < -0.5\text{) then mask} \quad (2)$$

Only nadir images with satellite viewing angle $<35^{o}$ were considered, in order to minimize angular effects from bidirectional reflectivity in heterogeneous areas. The MRT images were compared with the MODIS surface reflectance products (MOD09: 8-day composite surface reflectance images) to establish a general level of consistency, as well as with field surface reflectances from the multispectral radiometer.

3.2. Aerosol retrieval

The satellite measures aerosol reflectances, which are decomposed from TOA reflectances, surface reflectances, and Rayleigh reflectance (Eq. (1)). This can then be fitted to values calculated from known aerosol optical properties to derive the AOT from the image wavelengths. The Santa Barbara DISORT Radiative Transfer (SBDART; Ricchiazzi et al., 1998) model was used for constructing the LUT. Cluster analysis was used to classify natural and anthropogenic aerosols using 24 parameters from the AERONET level 2 aerosol and inversion products (Holben et al, 1998), which include AOT (τ_{500}), angstrom exponent ($\alpha_{870-440}$) value, 4 single scattering albedo values, 8 real and imaginary refractive index values, 4 asymmetry factor values, 2 mean radius values, 2 standard deviation values, and 2 mode total volume values. The data points are allocated to groups according to their associations with the nearest centroid. In this study, the number of clusters was first tested by Ward's automated hierarchical clustering method (Ward, 1963), which calculate the distance between each step from 0 to 730 (the sample of data). The "elbow" or "saturation" point was found at step 726. Therefore, the number of clusters was set as four (730–726 = 4). Sensitivity tests were carried out to examine the appropriate number of classes, using the distance between cluster centers, the variability of cluster membership, and 2D/3D scatter plots to demonstrate the separability and robustness of the four clusters (Wong, 2009).

Table 2
Summary of step sizes of the input parameters in LUT.

Parameter	Node
AOT	0, 0.2, 0.4, 0.8, 1, 1.5, 2, 2.5, 3, 3.5, 4, 5
Solar zenith angle	0~80° (Δ = 10°)
Viewing zenith angle	0~80° (Δ = 5°)
Azimuth angle	0~170° (Δ = 10°)
Bands	MODIS 3 bands (470, 550, 660 nm)
Aerosol models	4 Types

Four characteristic aerosol types were defined using a total of 730 cases during 2005 to 2008. They are (i) coastal urban, (ii) polluted urban, (iii) dust (likely to be long distance desert dust, Wong et al. (2010)), and (iv) heavy pollution. Table 1 shows the aerosol and microphysical properties, as well as the number of records for each cluster. The 2D/3D scatter plots are given in Wong (2009).

For the clustering, type 1 (coastal urban) has the largest number of records (45% of total) and type 3 (dust) has the least (3% of total). This indicates that the Hong Kong AERONET station is most affected by urban pollution, and least by desert dust due to the long distance from the source area in north China. Heavy urban pollution (type 4) accounts for 22% of the total records, and type 2 (polluted urban aerosol) accounts for 30%. In this classification, there is no cluster representing rural and background aerosol types in Hong Kong, since the AERONET station is deployed in the urban area.

Type 1 (coastal urban) has moderate absorption properties (Single Scattering Albedo (SSA) at 0.44 μm = 0.88 (Table 1)), and it is dominated by both coarse and fine particles (Fig. 3), of which the coarse mode most likely

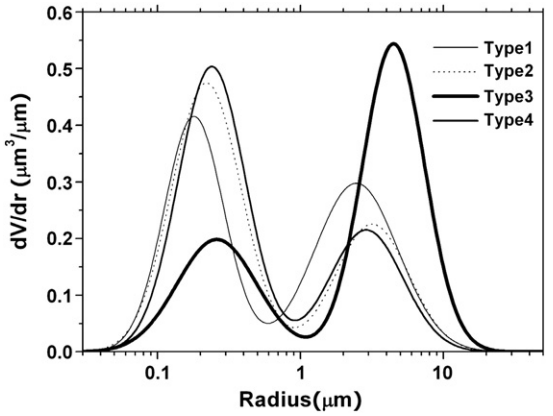

Fig. 3. Aerosol size (log-normal) distributions used in this study. Types 1, 2, 3, 4 represent coastal urban, polluted urban, dust, and heavy pollution aerosols, respectively.

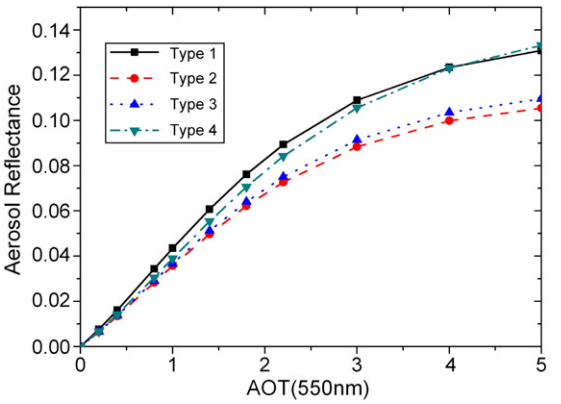

Fig. 4. Look Up Table for aerosol reflectance against AOT. The SBDART calculations were performed with solar zenith = 30°, satellite zenith angle = 10°, azimuth angle = 150°.

Table 3
AOT retrieval errors caused by sensor calibration, Rayleigh scattering, SSA, and asymmetry factor.

Parameter	Calibration	Rayleigh scattering	SSA	Asymmetry factor
Control factor	5%	5%	5%	5%
dAOT	0.085	0.045	0.28	0.15
dAOT(%)	5.2%	4.63%	12.25%	9.94%

originates from marine aerosols (since the AERONET is located only 1 km from the coast) and the fine mode from local urban pollutants. The moderate absorption properties of this type could be due to the proportion of carbonaceous particles, which have high absorption properties, in urban pollutants (Torres et al., 2005; Bergstrom et al., 2007). Type 2 (polluted urban) also has moderate absorption properties (SSA at 0.44 μm = 0.87) and a high volume of fine particles (0.081) (Table 1). Type 2 (polluted urban) and type 4 (heavy pollution) show a similar size distribution (Fig. 3), but type 2 has lower AOT (0.52). Dust (type 3) exhibits relatively high AOT ($\tau_{500} = 0.51$) with a large amount of coarse particles (68% of total volume concentration). Heavy pollution (type 4) is characterized by high aerosol concentrations ($\tau_{500} > 1$) and a large volume of fine particles (70%) and mainly represents fine particles from local traffic emission occurring on days with low wind speeds and/or inversion conditions.

Although Sifakis et al. (1998) found that when relative humidity levels exceed 60%, water vapor does contribute to visibility reduction and AOT, the humidity factor in the growth of aerosol size has already been accounted for by the microphysical properties in the clustering.

For the LUT construction, the above 4 aerosol models with 9 solar zenith angles (0–80°, $\Delta = 10°$), 17 view zenith angles (0–80°, $\Delta = 5°$), 18 relative sun/satellite azimuth angles (0–170°, $\Delta = 10°$) were considered. The SBDART code uses the aerosol properties associated with a given model, plus the combinations of values for the 3 parameters listed above (amounting to 33048 combinations for 3 bands (470, 550, 660 nm)), to compute the hypothetical AOT. Table 2 shows the step sizes of the input parameters in the LUT. The original LUT contained the AOT values and TOA reflectances for different geometries, while LUTs of aerosol reflectances as a function of AOT values at different geometries were also created by Eq. (3):

$$\rho_{Aer} = \rho_{TOA} - \rho_{TOA\_when\_AOT=0} \tag{3}$$

Table 5
Statistical comparisons between the surface reflectance of MRT with multispectral radiometer data. RMS (root mean square) and MAD (mean absolute differences) errors in 470, 550, 660 nm.

	470 nm	550 nm	660 nm
RMS error	0.0339	0.0488	0.0533
MAD error	0.0309	0.0268	0.0293

where ρ_{Aer} is aerosol reflectance, ρ_{TOA} is TOA reflectance, $\rho_{TOA\_when\_AOT=0}$ is the TOA reflectance when AOT = 0, it also is Rayleigh reflectance. Fig. 4 represents one of the LUTs from the SBDART results.

For the sensitivity analysis of AOT retrieval, the parameters of sensor calibration, aerosol optical properties (SSA, asymmetry factor), and Rayleigh scattering from the above 4 aerosol models were considered. The sensitivity analysis for each of the retrieval-related factor is summarized in Table 3. From Table 3, the MODIS sensor calibration uncertainty referenced from the MODIS Level 1B product user's guide is ca. 1.5–5%. The resulting SSA and asymmetry factor retrieval errors are comparative large: 0.28, 0.15 (12.25%, 9.94%), respectively. Another small error may be incurred by Rayleigh scattering. Rayleigh scattering error can cause an error of 0.045 (4.63%).

Before deriving aerosol reflectances from images, interpolation of the LUT geometry to the measured (satellite) geometry was undertaken. The bilinear interpolation method was adopted for interpolating between two nearest data in LUTs at a given geometry. This step can reduce the number of LUT values being read in the computer memory. Then the image aerosol reflectances can be calculated using Eq. (1), and the modeled aerosol reflectance can be searched from LUTs. Finally, the satellite observed aerosol reflectances ($\rho_{\lambda_j}{}^a$) were compared to the modeled aerosol reflectances ($\rho_{\lambda_j}{}^m$) for each geometrically corrected LUT. For these comparisons, an optimal spectral shape-fitting technique was executed to select the aerosol model with the smallest systematic errors (Kaufman and Tanré, 1998; Torricella et al., 1999; Lee et al., 2007) (Eq. (4)).

$$x^2 = \frac{1}{n}\sum_{i=1}^{n}\left(\frac{\rho_{\lambda_j}^m - \rho_{\lambda_j}^a}{\rho_{\lambda_j}^m}\right)^2 \tag{4}$$

The error term of x^2 is described as the residual of the measured aerosol reflectances $\rho_{\lambda_j}^m$ from MODIS and modeled aerosol reflectances $\rho_{\lambda_j}^a$ from aerosol models in three different wavelengths (e.g., 470, 550, 660 nm). The minimum residual of x^2 is selected from the four aerosol types for each pixel.

Table 4
Statistical comparisons between the surface reflectance of MRT with MOD09 product. RMS (root mean square) and MAD (mean absolute differences) errors in 470, 550, 660 nm over winter, autumn, and spring seasons.

	Winter			Autumn			Spring		
	470 nm	550 nm	660 nm	470 nm	550 nm	660 nm	470 nm	550 nm	660 nm
RMS error	0.0202	0.0097	0.0114	0.0260	0.0097	0.0140	0.0170	0.0152	0.0146
MAD error	0.0191	0.0070	0.0083	0.0249	0.0080	0.0120	0.0150	0.0109	0.0106

After locating the appropriate aerosol model, the AOT values at 470 nm, 550 nm, and 660 nm were derived for each pixel.

4. Results

4.1. Reliability of surface reflectance

Strong correlations in surface reflectance values were obtained between the MRT images and MOD09 surface reflectance product for the fall and winter seasons ($r^2 > 0.87$), while moderate correlations were noted in the spring season ($r^2 > 0.76$). These were obtained from random sampling of vegetated, urban, grassland, and shrubland areas over the whole of Hong Kong and the Pearl River Delta region. The largest mean absolute differences and greatest root mean square errors were obtained for shorter wavelengths such that the MADs for the 470 nm, 550 nm, and 660 nm wavebands bands were ca. 0.0249, 0.0109, and 0.0120, and the RMS errors were 0.0260, 0.0152, and 0.0146, respectively (Table 4).

For fifty-one ground-based reflectance measurements from the multispectral radiometer taken on four winter dates (Table 5), the general differences between minimum reflectances from the winter MRT images and ground reflectances were between 0.01 and 0.03 (i.e., 1–3% reflectance units). The MAD values were 0.031 (470 nm), 0.027 (550 nm), and 0.029 (660 nm), respectively (Table 5). Since ground-based measurements were only taken from vegetated areas, there were no check points on bright and dark urban surfaces. The error of our field reflectances was of similar magnitude to the error of surface reflectances given for MOD09, i.e., 0.025. When this magnitude of error due to surface reflectance is translated into AOT using SBDART (a radiative transfer model which allocates AOT values to the derived aerosol reflectances, the AOT error due to error in surface reflectance is between 0 and 0.30.

4.2. Validation of derived AOT

The MODIS 500 m retrieved AOT was validated using AERONET measurements for 2007 (Fig. 5a) and a good agreement ($r^2 = 0.767$) is shown between our methodology and the AERONET. By comparison, the MOD04 collection 4 and 5 AOT data at 10 km resolution (Fig. 5b) obtained correlation coefficients of $r^2 = 0.671$ and $r^2 = 0.778$ for collection 4 and collection 5, respectively. The correlation coefficient of our methodology is in between the values of collection 4 and 5. Most importantly, the methodology retrieves AOT images at a much higher spatial resolution and can thus show detailed AOT levels over both bright urban and dark rural vegetated areas. This improvement is significant for a topographically complex area like Hong Kong.

A good agreement was shown between AOT from Microtops II measurements and AOT derived from MODIS 500 MRT images, with a correlation coefficient $r^2 = 0.760$ (Fig. 5c). The MAD error between MODIS 500 m AOT and Microtops II is 0.150, whereas a smaller MAD error (0.142) was obtained for the comparison with AERONET. An RMS error of 0.182 was obtained from Microtops II, whereas a smaller RMS error (0.176) was obtained for the comparison with AERONET. In general, the MAD and RMS errors can be said to represent an error range between 0.150 and 0.182 in AOT values, which is a satisfactory result as it is smaller than the range of error in AOT attributable to uncertainty of the surface reflectances (0–0.30).

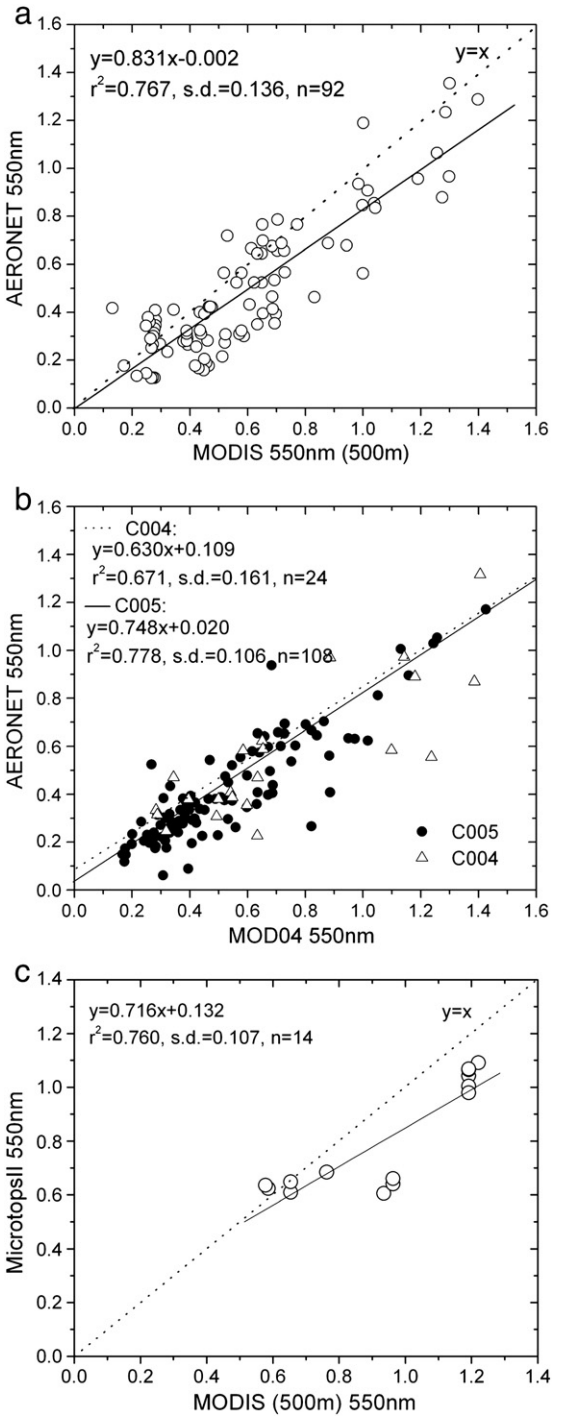

Fig. 5. Scatter plots (a) between MODIS 500 m AOT and AERONET measurements; (b) between MOD04 collection 4, 5 AOT and AERONET measurements; (c) between MODIS 500 m AOT and Microtops II measurements.

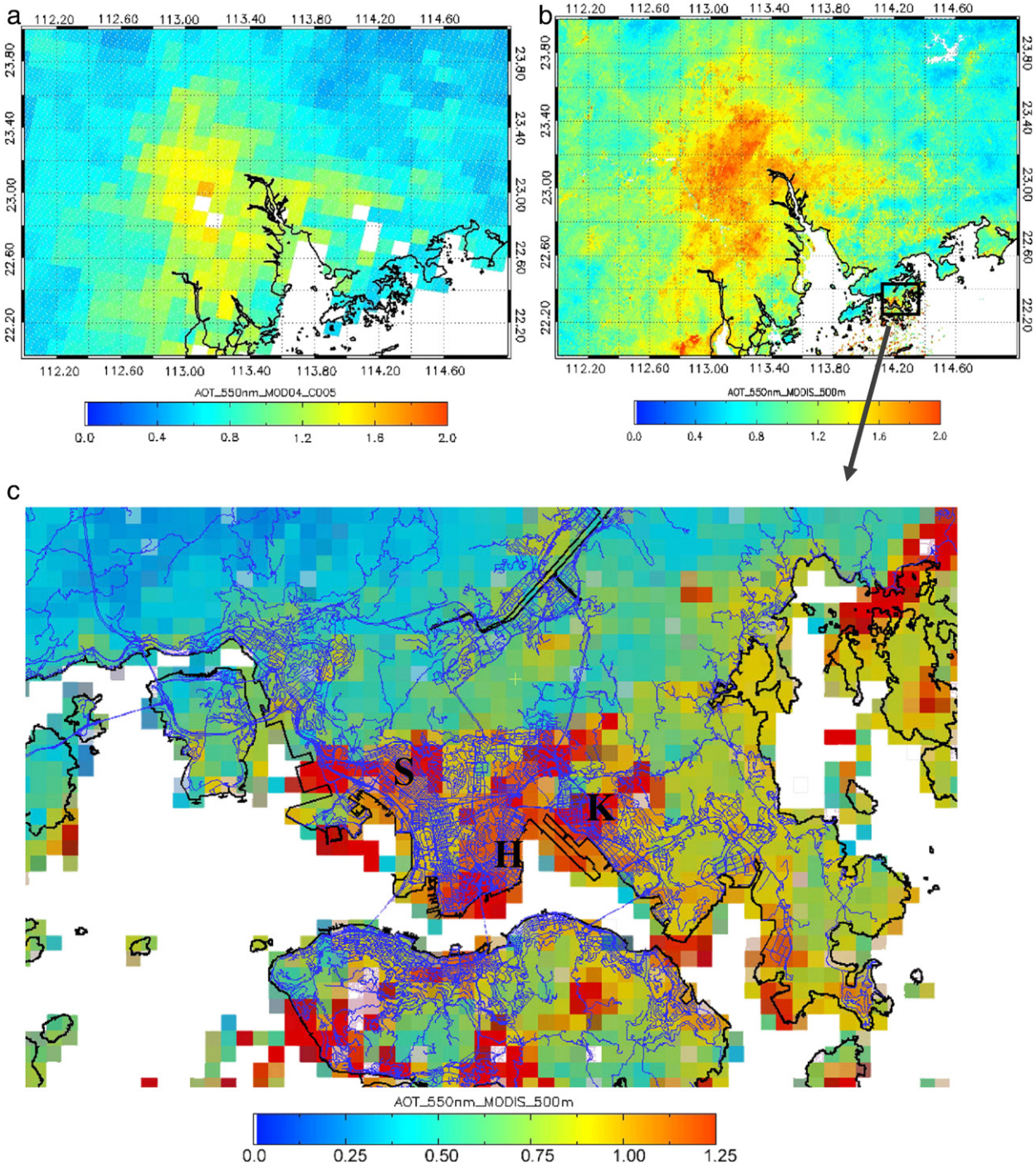

Fig. 6. AOT images (a) at 550 nm derived from MODIS collection 5 algorithm; (b) from this study with 500-m resolution over Hong Kong and the Pearl River Delta region; (c) overlaid with GIS road data.

5. Applications of fine resolution AOT images

5.1. Characterization of spatial pattern of AOT

The AOT distribution over Hong Kong and the PRD region on Oct. 20, 2007, retrieved using MODIS collection 5 at 10 km, and the MRT images at 500 m are shown in Fig. 6. About fifteen pixels cover the entire Hong Kong territories with an AOT image at 10 km resolution (Fig. 6a), while there are about 300 using 500 m resolution (Fig. 6b). Therefore, the spatial pattern of aerosols especially in Shenzhen (the Chinese city adjacent to Hong Kong) is much more precisely defined using the 500 m

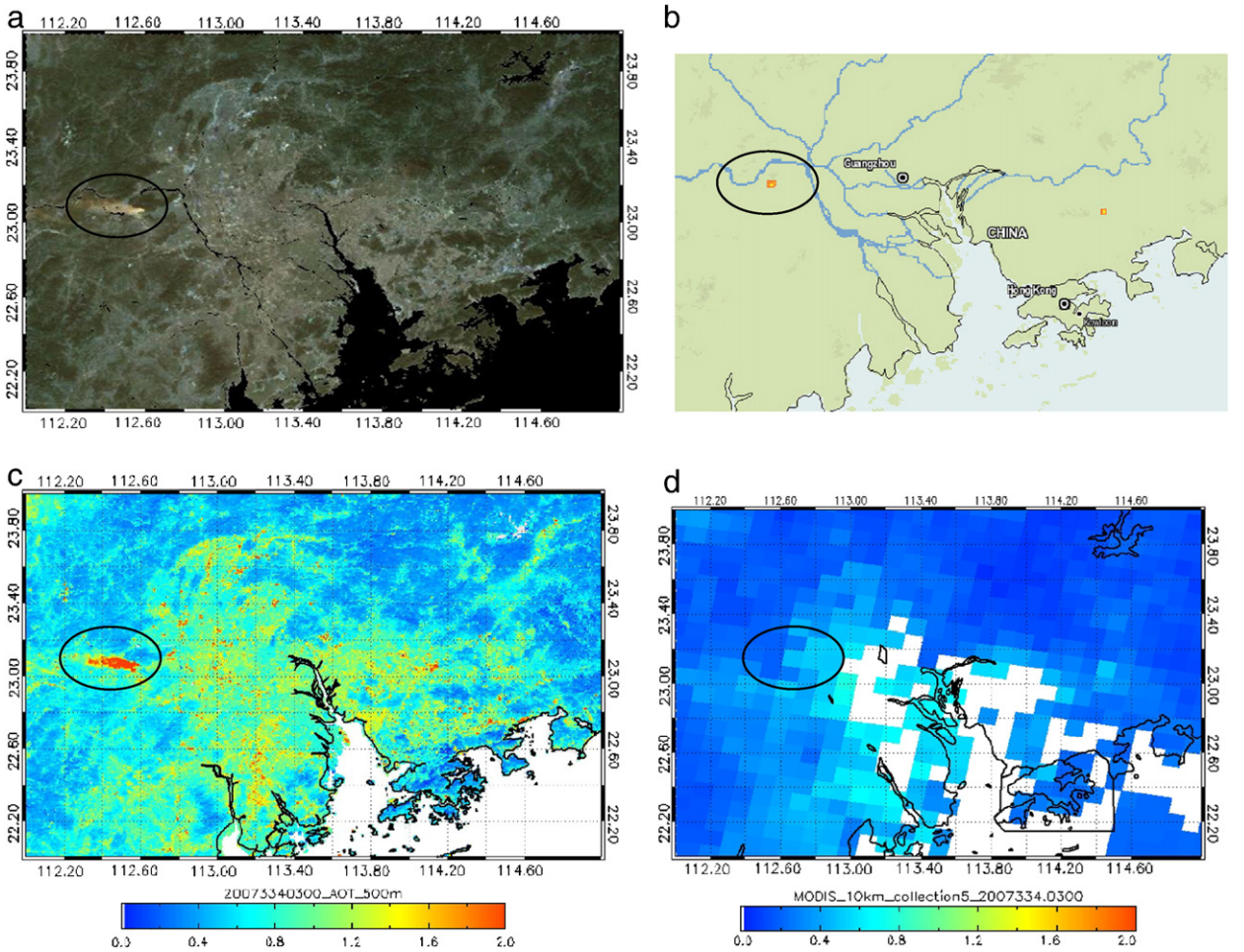

Fig. 7. (a) Rayleigh corrected RGB image on Nov. 30, 2007; (b) fire spots shown on Nov. 30, 2007 from the Web Fire Mapper (courtesy of the Geography Department of the University of Maryland); (c) AOT 500 m image; (d) AOT collection 5 10 km image.

AOT image compared with the 10 km coarse pixels of MOD04. Fig. 6c shows the 500 m AOT images over Kowloon peninsula and part of Hong Kong island overlaid with GIS road networks. Dense urban and commercial districts like Hung Hom (H), Sham Shui Po (S), and Kowloon Bay (K) observe high AOT values (~1.0), whereas the rural areas have relatively low AOT values (~0.3). Such steep aerosol gradients indicated by the 500 m MRT images are plausible for this region, with tens of thousands of polluting industries located around Shenzhen but almost none on the Hong Kong side of the border. Within Hong Kong, aerosols generated by local traffic are spatially constrained by the extremely high rise nature of the built environment, with deep street canyons, and precipitious slopes at the urban periphery. Additionally, Section 5.2 indicates a small smoke plume due to biomass burning that can be resolved at 500 m resolution, further indicating the heterogeneity of aerosol patterns in the region.

5.2. Aerosols from biomass burning in south China

China is still an agricultural country and had a yield of 690 million tons of straw in 2000 (Wang et al., 2007), of which 36% is used for domestic fuel and 7% is disposed by open fires (Gao et al., 2002). In the forested region of the Pearl River Delta, biomass burning, both intentional and accidental, occurs frequently. Locating and mapping the fire sources is possible using MODIS 500 m AOT images as the smoke plumes can be resolved.

Fig. 7a shows the Rayleigh corrected MODIS RGB image on Nov. 30, 2007. Biomass burning clearly evident on the left of the image (marked on the image), which is located in the dense forest area of Zhaoqing county. High AOT values (>1.8) are observed with MODIS 500 m AOT image (Fig. 7c). The smoke plumes and the source of burning can be easily identified on the 500 m AOT image, whereas it is not observable on the MODIS 10 km AOT image. In addition, a large patch of the urban areas are masked out with no AOT data values on MODIS collection 5 algorithm (Fig. 7d) due to their high surface reflectances, which are not meeting the surface reflectance criteria in the collection 5 AOT algorithm. Fig. 7b shows the same fire spots located from the Web Fire Mapper developed by the Geography Department of the University of Maryland (Justice et al., 2002). Also the easterly wind that was blowing confirmed the direction of the smoke plume.

6. Discussion and conclusion

The Minimum Reflectance Technique coupled with "in situ" aerosol models based on the Hong Kong AERONET data and sun-satellite geometries is able to accurately retrieve aerosols over both urban and vegetated areas at a level of detail, which is higher than previous MODIS AOT products. The MODIS 500 m AOT images derived from the MRT technique show a high level of accuracy ($r^2 = 0.767$, RMS error = 0.176, MAD error = 0.142) compared with ground-based measurements, similar to the stated accuracies of the MODIS operational 10 km products. The similar accuracy is probably because the same AERONET, in the center of the urban area of Hong Kong, was used for validating both algorithms. Since this is an extremely densely urbanized region, there is little variation in aerosol concentrations over the whole region, i.e., little variation over 500 m and 10 km. Although the signal-to-noise ratio of the 10 km resolution data is 20 times higher than the 500 m resolution data (Kaufman and Tanré, 1998), Henderson and Chylek (2005) found that there are only small changes in aerosol estimates with increasing pixel sizes from 40×80 m^2 to 2040×4080 m^2, and the AOT differences are even negligible. Therefore, any loss of accuracy due to a decreased signal-to-noise ratio of the 500 m AOT may be small, or is small enough to be compensated by increased accuracy due to the higher resolution when validated against AERONET data.

The thresholding adopted by this study for cloud removal was tested by a trial-and-error approach. When compared with the cloud cover data from the Hong Kong Observatory, an accuracy of 78.13% was achieved, which is comparable to the 82% accuracy from the MODIS operational algorithm. The errors are caused from small cirrus clouds present on the images, and they may easily be confused with bright urban surfaces. In addition, cloud shadow is difficult to mask except by using very high resolution thermal images. Even though collection 4 and 5 algorithms make use of the MODIS 1 km thermal band for detecting and masking the clouds, sometimes, the AOT end products show large patches of very high AOT over the sea, which is an error caused by incomplete cloud masking. Therefore, more analysis and tests will be conducted in future work.

Given the high accuracy and high spatial resolution of the 500 m AOT images produced in this study, they can be used to study daily aerosol distributions from localized intra-urban emissions, transient cross-boundary sources, and biomass burning events. The aerosol retrieval methodology presented here can be transferred to other Asian cities such as Taipei and Singapore, with similar climatic and meteorological conditions.

Acknowledgments

The authors would like to acknowledge the NASA Goddard Earth Science Distributed Active Archive Center for the MODIS Level IB and Level 2 data and Brent Holben for helping with the Hong Kong PolyU AERONET station. Grant PolyU 5253/07E from the RGC and PolyU PDF research grant G-YX1W sponsored the research. The research of K. H. Lee was supported by the Korea Meteorological Administration Research and Development Program under Grant RACS-2010-1003.

Appendix. Derivation of Rayleigh surface

The determination of Rayleigh path radiance was based on the computation of spectral dependence of the Rayleigh optical depth and phase function. The Bucholtz (1995) equation (Eq. (5)) was adopted for calculating the Rayleigh scattering optical thickness:

$$\tau_{Ray}(\lambda) = A \cdot \lambda^{-(B+C\lambda+D/\lambda)} \times \frac{p(z)}{p_0} \tag{5}$$

where A, B, C, D are the constants of the total Rayleigh scattering cross-section and the total Rayleigh volume scattering coefficient at standard atmosphere. $p(z)$ is the pressure (hPa) relevant to the height, which was determined by the parameterized barometric equation.

$$p(z) = p_0 \cdot exp\left[\frac{-29.87 \cdot g \cdot 0.75 \cdot z}{8.315 \cdot (T_{SURF} - g \cdot 0.75 \cdot z)}\right] \tag{6}$$

where g is the gravity acceleration (9.807 ms^{-2}), T_{surf} is the surface temperature (acquired from the Hong Kong Observatory) (e.g., 298 K) and p_0 is the actual pressure in mean sea level (1008 hPa) and z is the height (m). A Digital Elevation Model (DEM) in MOD03 geolocation data was used for estimating the height z and for calculating the pressure $p(z)$ for each pixel.

References

Bergstrom, R.W., Pilewskie, P., Russell, P.B., Redemann, J., Bond, T.C., Quinn, P.K., Sierau, B., 2007. Spectral absorption properties of atmospheric aerosols. Atmos. Chem. Phys. 7, 5937–5943. doi:10.5194/acp-7-5937-2007.

Bucholtz, A., 1995. Rayleigh-scattering calculations for the terrestrial atmosphere. Appl. Opt. 34, 2765–2773.

Chang, J., Clay, S.A., Clay, D.E., Aaron, D., Helder, D., Dalsted, K., 2005. Clouds influence precision and accuracy of ground-based spectroradiometers. Commun. Soil Sci. Plant Anal. 36 (13–14), 1799–1807.

Chu, A., Kaufman, Y.J., Ichoku, C., Remer, L.A., Tanré, D., Holben, B.N., 2002. Validation of MODIS aerosol optical depth retrieval over land. Geophys. Res. Lett. 29 (12), 1–4.

Deschamps, P.Y., Herman, M., Lenoble, J., Tanré, D., Viollier, M., 1980. Atmospheric effects in remote sensing of ground and ocean reflectances. Remote Sensing of Atmosphere and Ocean. Academic Press, New York, pp. 115–148.

Gao, X.Z., Ma, W.Q., Ma, C.B., Zhang, F.S., Wang, Y.H., 2002. Analysis on the current status of utilization of crop straw in China. J. Huazhong Agric. Univ. 21, 242–247.

Henderson, B.G., Chylek, P., 2005. The effect of spatial resolution on satellite aerosol optical depth retrieval. IEEE Trans. Geosci. Remote Sens. 43 (9), 1984–1990.

Herman, J.R., Celarier, E.A., 1997. Earth surface reflectivity climatology at 340–380 nm from TOMS data. J. Geophys. Res. 102, 28003–28011.

Holben, B.N., Eck, T.F., Slutsker, I., Tanré, D., Buis, J.P., Setzer, A., Vermote, E.F., Reagan, J.A., Kaufman, Y.J., Nakajima, T., Lavenu, F., Jankowiak, I., Smirnov, A., 1998. AERONET-A federated instrument network and data archive for aerosol characterization. Remote Sens. Environ. 66 (1), 1–16.

Hsu, N.C., Tsay, S.C., King, M.D., Herman, J.R., 2004. Aerosol properties over bright-reflecting source regions. IEEE Trans. Geosci. Remote Sens. 42 (3), 557–569.

Ichoku, C., Chu, D.A., Mattoo, S., Kaufman, Y.J., Remer, L.A., Tanré, D., Slusker, I., Holben, B.N., 2002. A spatio-temporal approach for global validation and analysis of MODIS aerosol products. Geophys. Res. Lett. 29, 8006. doi:10.1029/2001GL013206.

Justice, C.O., Giglio, L., Korontzi, S., Owens, J., Morisette, J.T., Roy, D.P., Descloitres, J., Alleaume, S., Petitcolin, F., Kaufman, Y., 2002. The MODIS fire products. Remote Sens. Environ. 83, 244–262.

Kaufman, Y.J., Tanré, D., Gordon, H.R., Nakajima, T., Lenoble, J., Frouin, R., Grassl, H., Herman, B.M., King, M.D., Teillet, P.M., 1997b. Passive remote

sensing of tropospheric aerosol and atmospheric correction for the aerosol effect. J. Geophys. Res. 102 (D14), 16815–16830.
Kaufman, Y.J., Tanré, D., Remer, L.A., Vermote, E.F., Chu, A., Holben, B.N., 1997a. Operational remote sensing of tropospheric aerosol over land from EOS Moderate Resolution Imaging Spectroradiometer. J. Geophys. Res. 102 (D14), 17051–17067.
Kaufman, Y.J., Tanré, D., 1998. Algorithm for remote sensing of tropospheric aerosol from MODIS. A Report from NASA MOD04 product - Algorithm Theoretical Basis Documents. NASA, United States, pp. 26–51.
King, M.D., Kaufman, Y.J., Tanré, D., Nakajima, T., 1999. Remote sensing of tropospheric aerosols from space: past, present, and future. Bull. Am. Meteorol. Soc. 80, 2229–2259.
Koelemeijer, R.B.A., de Haan, J.F., Stammes, P., 2003. A database of spectral surface reflectivity in the range 335–772 nm derived from 5.5 years of GOME observations. J. Geophys. Res. 108, 4070.
Lee, K.H., Kim, Y.J., von Hoyningen-Huene, W., Burrow, J.P., 2007. Spatio-temporal variability of atmospheric aerosol from MODIS data over Northeast Asia in 2004. Atmos. Environ. 41 (19), 3959–3973.
Lee, K.H., Li, Z., Kim, Y.J., Kokhanovsky, A., 2009. Aerosol monitoring from satellite observations: a history of three decades. In: Kim, Y.J., Platt, U., Gu, M.B., Iwahashi, H. (Eds.), Atmospheric and Biological Environmental Monitoring.
Levy, R.C., Remer, L.A., Martins, J.V., Kaufman, Y.J., Plana-fattori, A., Redemann, J., Wenny, B., 2004. Evaluation of the MODIS aerosol retrievals over ocean and land during CLAMS. J. Atmos. Sci. 62 (4), 974–992.
Levy, R.C., Remer, L.A., Mattoo, S., Vermote, E.F., Kaufman, Y.J., 2007. Second-generation operational algorithm: retrieval of aerosol properties over land from inversion of Moderate Resolution Imaging Spectroradiometer spectral reflectance. J. Geophys. Res. 112, D13211.
Li, C.C., Lau, A.K.H., Mao, J.T., Chu, D.A., 2005. Retrieval, validation, and application of the 1-km aerosol optical depth from MODIS measurements over Hong Kong. IEEE Trans. Geosci. Remote Sens. 43 (11), 2650–2658.
Li, Z., Niu, F., Lee, K.H., Xin, J., Hao, W.M., Nordgren, B., Wang, Y., Wang, P., 2007. Validation and understanding of Moderate Resolution Imaging Spectroradiometer aerosol products (C5) using ground-based measurements from the handheld Sun photometer network in China. J. Geophys. Res. 112, D22S07.
Mi, W., Li, Z., Xia, X.G., Holben, B., Levy, R., Zhao, F.S., Chen, H.B., Cribb, M., 2007. Evaluation of the MODIS aerosol products at two AERONET stations in China. J. Geophys. Res. 112, D22S08.
Otterman, J., Fraser, R.S., 1979. Adjacency effects on imaging by surface reflection and atmospheric scattering: cross radiance to zenith. Appl. Opt. 18, 2852–2860.
Remer, L.A., Kaufman, Y.J., Tanré, D., Mattoo, S., Chu, D.A., Martins, J.V., Li, R.-R., Ichoku, C., Levy, R.C., Kleidman, R.G., Eck, T.F., Vermote, E., Holben, B.N., 2005. The MODIS aerosol algorithm, products and validation. J. Atmos. Sci. 62 (4), 947–973.
Ricchiazzi, P., Yang, S.R., Gautier, C., Sowle, D., 1998. SBDART: a research and teaching software tool for plane-parallel radiative transfer in the Earth's atmosphere. Bull. Am. Meteorol. Soc. 79 (10), 2101–2114.
Sifakis, N., Soulakellis, N.A., Paronis, D.K., 1998. Quantitative mapping of air pollution density using earth observations: a new processing method and applications to an urban area. Int. J. Remote Sens. 19, 3289–3300.
Tanré, D., Herman, M., Deschamps, P.Y., De Leffe, A., 1979. Atmospheric modeling for space measurements of ground reflectances, including bidirectional properties. Appl. Opt. 18, 3587–3594.
Torres, O., Bhartia, P.K., Sinyuk, A., Welton, E.J., Holben, B., 2005. Total Ozone Mapping Spectrometer measurements of aerosol absorption from space: comparison to SAFARI 2000 ground-based observations. J. Geophys. Res. 110, D10S18. doi:10.1029/2004JD004611 2005.
Torricella, F., Cattani, E., Cervino, M., Guzzi, R., Levoni, C., 1999. Retrieval of aerosol properties over the ocean using global ozone monitoring experiment measurements: method and applications to test cases. J. Geophys. Res. 104 (10), 12085–12098.
Vermote, E.F., El Saleous, N.Z., 2006. Operational atmospheric correction of MODIS visible to middle infrared land surface data in the case of an infinite lambertian *target*. In: Qu, J., et al. (Ed.), Earth Science Satellite Remote Sensing, Science and Instruments, 1, pp. 123–153 (8).
Wang, Q., Shao, M., Liu, Y., William, K., Paul, G., Li, X., Liu, Y., Lu, S., 2007. Impact of biomass burning on urban air quality estimated organic tracers: Guangzhou and Beijing as cases. Atmos. Environ. 41, 8380–8390.
Ward, J.H., 1963. Hierachical grouping to optimize an objective function. J. Am. Stat. Assoc. 58, 236–244.
Wong, M.S., Lee, K.H., Nichol, J.E., Li, Z.Q., 2008. Retrieval of aerosol optical thickness using MODIS 500 × 500m^2, a study in Hong Kong and Pearl River Delta region. Proceedings of International Workshop on Earth Observation and Remote Sensing Applications, Jun 30– Jul 2, 2008, Beijing, China. doi:10.1109/EORSA.2008.4620353.
Wong, M.S., 2009. Retrieval of Aerosol Optical Thickness at 500 m resolution using MODIS images, a study in Hong Kong and the Pearl River Delta region. Ph.D. thesis, The Hong Kong Polytechnic University, Hong Kong, pp. 53–67.
Wong, M.S., Nichol, J.E., Holben, B., 2010. Desert dust observed in a humid tropical city: Hong Kong. Int. J. Remote Sens. 31 (4), 1043–1051.